NeuroImage 143 (2016) 70–81

Contents lists available at ScienceDirect

NeuroImage

journal homepage: www.elsevier.com/locate/neuroimage

Resting state network topology of the ferret brain

Zhe Charles Zhou [a,h], Andrew P. Salzwedel [i,j], Susanne Radtke-Schuller [a], Yuhui Li [a], Kristin K. Sellers [a,h], John H. Gilmore [a], Yen-Yu Ian Shih [c,d,e,f,g,h], Flavio Fröhlich [a,b,c,d,g,h,*,1,2], Wei Gao [i,j,**,1]

[a] Department of Psychiatry, University of North Carolina at Chapel Hill, Chapel Hill, NC 27599, United States
[b] Department of Cell Biology and Physiology, University of North Carolina at Chapel Hill, Chapel Hill, NC 27599, United States
[c] Department of Biomedical Engineering, University of North Carolina at Chapel Hill, Chapel Hill, NC 27599, United States
[d] Department of Neurology, University of North Carolina at Chapel Hill, Chapel Hill, NC 27599, United States
[e] Biomedical Research Imaging Center, University of North Carolina at Chapel Hill, Chapel Hill, NC 27599, United States
[f] Small Animal Imaging Facility, University of North Carolina at Chapel Hill, Chapel Hill, NC 27599, United States
[g] Neuroscience Center, University of North Carolina at Chapel Hill, Chapel Hill, NC 27599, United States
[h] Neurobiology Curriculum, University of North Carolina at Chapel Hill, Chapel Hill, NC 27599, United States
[i] Biomedical Imaging Research Institute, Cedars-Sinai Medical Center, Los Angeles, CA 90048, United States
[j] Department of Biomedical Sciences, Cedars-Sinai Medical Center, Los Angeles, CA 90048, United States

ARTICLE INFO

Article history:
Received 5 May 2016
Accepted 1 September 2016
Available online 2 September 2016

Keywords:
Resting state
fMRI
Ferret
Default mode network
Networks
Graph theory

ABSTRACT

Resting state functional magnetic resonance imaging (rsfMRI) has emerged as a versatile tool for non-invasive measurement of functional connectivity patterns in the brain. RsfMRI brain dynamics in rodents, non-human primates, and humans share similar properties; however, little is known about the resting state functional connectivity patterns in the ferret, an animal model with high potential for developmental and cognitive translational study. To address this knowledge-gap, we performed rsfMRI on anesthetized ferrets using a 9.4 T MRI scanner, and subsequently performed group-level independent component analysis (gICA) to identify functionally connected brain networks. Group-level ICA analysis revealed distributed sensory, motor, and higher-order networks in the ferret brain. Subsequent connectivity analysis showed interconnected higher-order networks that constituted a putative default mode network (DMN), a network that exhibits altered connectivity in neuropsychiatric disorders. Finally, we assessed ferret brain topological efficiency using graph theory analysis and found that the ferret brain exhibits small-world properties. Overall, these results provide additional evidence for pan-species resting-state networks, further supporting ferret-based studies of sensory and cognitive function.

Introduction

Behavior and cognition are supported by the brain's intrinsic anatomical and functional connectivity (i.e. correlated activity patterns between distinct brain regions) (Fox et al., 2012; Brusa et al., 2014; Zhou et al., 2016a). Resting state functional magnetic resonance imaging (rsfMRI) has emerged as a powerful tool for measuring functional connectivity non-invasively across species (Biswal et al., 1995; Damoiseaux et al., 2006; Vincent et al., 2007; Belcher et al., 2013; Mechling et al., 2014; Kyathanahally et al., 2015). Groups of functionally connected brain regions measured using rsfMRI can be defined as networks that likely reflect the underlying structural organization and communication in the brain (Greicius et al., 2009; van den Heuvel and Hulshoff Pol, 2010). However, functional connectivity within such resting state networks (RSNs) is impaired in human psychiatric disorders such as schizophrenia, Alzheimer's disease, and autism spectrum disorders (Liu et al., 2008; Minshew and Keller, 2010; Sanz-Arigita et al., 2010; Zhang et al., 2011; Karbasforoushan and Woodward, 2012; Spetsieris et al., 2015; Wang et al., 2015). In particular, the default mode network (DMN), which is composed of hubs in the parietal and medial prefrontal cortices, exhibits elevated activity in neurotypical participants at rest, while the aforementioned disorders show either hypo- or hyperconnected DMNs (Raichle et al., 2001; Greicius et al., 2004; Minshew and Keller, 2010; Sheline et al., 2010; Wang et al., 2015). Resting state studies using graph theory analysis, a set of techniques that assesses information transfer among distributed brain regions, have suggested that human and animal brains exhibit small-world

* Correspondence to: 115 Mason Farm Rd, NRB 4109F, Chapel Hill, NC 27599, United States.
** Corresponding author at: Biomedical Imaging Research Institute, Cedars-Sinai Medical Center, Los Angeles, CA 90048, United States.
E-mail address: wei.gao@cshs.org (W. Gao).
[1] Authors contributed equally.
[2] flavio_frohlich@med.unc.edu.

http://dx.doi.org/10.1016/j.neuroimage.2016.09.003
1053-8119/

Nomenclature

18	area 18
19	area 19
20	area 20
20a	area 20a
20b	area 20b
21	area 21
A	amygdala
A1	primary auditory cortex
AAF	anterior auditory field
ac	anterior commissure
ADF	anterior dorsal field
AEG	anterior ectosylvian gyrus
ALLS	anteriolateral lateral suprasylvian cortex
AMLS	anterior medial lateral suprasylvian cortex
AON	anterior olfactory nucleus
AP	pretectal area
ASG	anterior sigmoid gyrus
AVF	anterior ventral field
cc	corpus callosum
Cb	cerebellum
CG	cingulate gyrus
CL	claustrum
CNG	coronal gyrus
dPFC	dorsal prefrontal cortex
f	fornix
Ent	entorhinal cortex
Hip	hippocampus
Hy	hypothalamus
IC	inferior colliculus
LG	lateral gyrus
LGN	lateral geniculate nucleus
LRSS	lateral bank of rostral suprasylvian sulcus
mPFC	medial prefrontal cortex
M1	primary motor cortex
MEG	medial ectosylvian gyrus
MGN	medial geniculate nucleus
MRSS	medial bank of rostral suprasylvian sulcus
NC	caudate nucleus
OB	olfactory bulb
och	optic chiasm
OBG	orbital gyrus, orbital cortex
opt	optic tract
PAG	periaqueductal grey
PEG	posterior ectosylvian gyrus
Pir	piriform cortex
PL	prelimbic cortex
PM	premotor cortex
PN	pontine nuclei
PPc	posterior parietal cortex, caudal part
PPF	posterior pseudosylvian field
PPr	posterior parietal cortex, rostral part
PRG	proreal gyrus
proCNG	CNG-like cortex bordering CNG rostrally
proPPF	PPF-like cortex bordering PPF rostrally
proPSG	PSG-like cortex bordering PSG rostrally
PSC	postsplenial cortex
PSSC	pseudosylvian sulcal cortex
PSF	posterior suprasylvian field
PSG	posterior sigmoid gyrus
RN	red nucleus
RSG	retrosplenial cortex
S1	primary somatosensory cortex
S2	secondary somatosensory cortex
S3	tertiary somatosensory cortex
SC	superior colliculus
S	septal nuclei
SN	substantia nigra
SSG	suprasylvian gyrus
SSy	suprasylvian cortex
Tha	thalamus
Tu	olfactory tubercle
VP	ventroposterior field
vPEG	ventral PEG

network topology (Watts and Strogatz, 1998; Achard et al., 2006; Bullmore and Sporns, 2012). This network attribute characterizes optimized trade-off between cost-efficient wiring and network resilience, and has shown to be altered in neuropsychiatric disorders (Liu et al., 2008; Zhang et al., 2011; Zhao et al., 2012).

Animal models bridge the gap between human psychiatric disorders and their underlying mechanisms. However, the study of these underlying mechanisms relies on accurate comparisons between animal model and human brain dynamics. Therefore, it is important to identify RSNs and their impairments across all research models. The ferret has a rich history of developmental research due to its early post-natal (P) ages corresponding to 25 weeks of gestation in the human (Barnette et al., 2009), as well as its short gestation time of ~42 days. Importantly, the ferret is born lissencephalic and the brain begins cortical folding (gyrification) at P10 (Sawada and Watanabe, 2012), allowing for translational study of early brain insults and impairments (Empie et al., 2015; Kou et al., 2015). Due to its well-developed sensory and higher-order brain structures, the ferret can be a useful model for studying sensory and cognitive impairments across a broad range of developmental time points (Basole et al., 2003; Fritz et al., 2010; Foxworthy et al., 2013a; Atiani et al., 2014). A map of neurotypical functional connectivity patterns would serve as a framework for translational studies in the ferret. Despite studies exploring the structure and function of individual brain regions, such large-scale brain network topology in the ferret has yet to be examined (Manger et al., 2002; Basole et al., 2003; Bizley and King, 2009; Fritz et al., 2010; Sellers et al., 2013; Bizley et al., 2015; Yu et al., 2015; Zhou et al., 2016b).

Here, we aimed to identify sensory and default mode RSNs in the ferret. We hypothesized that the ferret brain would exhibit RSNs comparable to those found in humans and non-human primates. To do this, we performed group-level independent component analysis (gICA), a data-driven approach to identify spatially independent functional networks, on anesthetized ferret resting state scans. Regions of interest composing the gICA functional networks were then compared to histological sections for identification of anatomical brain regions. Network connectivity measured by correlation analysis further validated within-network connectivity, and revealed the presence of interconnected somato-motor and putative default mode networks. We subsequently used graph theory analyses to demonstrate that the ferret brain network topology resembles that of a small-world network. As a whole, these findings add to the wealth of studies arguing for homologous cross-species RSNs (Vincent et al., 2007; Lu et al., 2012; Belcher et al., 2013; Hutchison et al., 2013; Mechling et al., 2014; Miranda-Dominguez et al., 2014; Sforazzini et al., 2014; Barks et al., 2015; Kyathanahally et al., 2015; Liang et al., 2015; Pan et al., 2015), and support the notion that ferrets are a robust animal model for translational research.

Materials and methods

Subjects

A total of six adult (16–19 weeks old) female ferrets (weighing 0.7 to 1 kg, group housed in a 12 h light/ 12 h dark cycle; Marshall BioResources, North Rose, NY) were included in this study. All animal procedures were performed in compliance with the National Institutes of Health guide for the care and use of laboratory animals (NIH Publications no. 8023, revised 1978), and approved by the Institutional Animal Care and Use Committee of the University of North Carolina at Chapel Hill and the United States Department of Agriculture (USDA Animal Welfare).

Animal preparation

Ferrets were initially anesthetized with intramuscular injection of ketamine/xylazine (30 mg/kg of ketamine, 1–2 mg/kg of xylazine) for subsequent intubation and setting of an intravenous (IV) line in the right saphenous vein. To control for the variability in eyelid position after anesthesia induction, the skin above and below the eyes were sutured individually such that the eyelids remained open throughout the scans. Lights within the scanner room were turned off for the duration of the experiment. The animal was then moved and placed into a custom-made, MRI-compatible stereotaxic holder. The holder was lined with a heating pad to maintain the rectal temperature of the animal at 38–39 °C. Animals were stabilized using custom ferret-compatible ear-bars and a tooth-bar. Animals were mechanically ventilated through an MRI compatible ventilator (0.5–0.75% isoflurane, 8–10cc, 50 bpm, medical grade air) and administered 5% dextrose lactated ringer's (4.264 mL/hr), xylazine (1.5 mg/kg/hr), and vecuronium bromide paralytic (0.0769 mg/kg/hr) via IV. The end-tidal CO_2 ($EtCO_2$; maintained around 3%), oxygen saturation, heart rate (estimated through the pulse oximeter), and rectal temperature were closely monitored throughout the procedure to ensure a stable plane of anesthesia. $EtCO_2$ values from this system were previously calibrated against invasive sampling of arterial blood gas in rats, reflecting a pCO_2 level of ~35 mmHg (Shih et al., 2012, 2013). Paralube and saline drops were applied to protect the eyes.

fMRI protocol

All data were acquired in a Bruker 9.4 T scanner (Bruker AVANCE, Billerica, MA). A 72 mm volume coil and four-channel phased array coil were used for excitation and signal reception, respectively. Anatomical images were acquired with the following Rapid Acquisition with Relaxation Enhancement (RARE) sequence: repetition time (TR)=3500 ms, echo time (TE)=35 ms, RARE factor=8, matrix size=280×280, FOV=2.8×2.8 cm^2, slice thickness=1 mm. Blood-oxygenation level dependent (BOLD) functional resting state scans were acquired with the following gradient-echo planar imaging (EPI) sequence: TR=2000 ms, TE=13 ms, matrix=80×80, field of view (FOV)=2.8×2.8 cm^2, slice thickness=1 mm. For both anatomical and functional scans, 24 adjacent slices were acquired with the same geometric positioning. Ten-minute resting state scans were acquired for all animals; for two animals, two additional resting state scans were acquired.

MR data pre-processing

Images were preprocessed using the Analysis of Functional NeuroImages software suite (AFNI v2011-12-21-1014, Bethesda, MD) and FMRIB's Software Libraries (FSL v5.0, University of Oxford, Oxford, UK). Briefly, the anatomical data workflow included removal of non-brain tissue (skull-stripping) and tissue segmentation. The anatomical data were skull-striped automatically (AFNI 3dautomask) and then hand-corrected for errors on a case-by-case basis. Tissue segmentation (FSL fast) was performed on the skull-stripped datasets to produce volumes representing cerebral spinal fluid (CSF) and white-matter (WM) for nuisance signal regression.

The functional data workflow included discarding volumes collected during scanner disequilibrium, slice-timing correction, motion correction, alignment to a pre-existing high-resolution T2-weighted template, spatial smoothing, band-pass filtering, and orthogonalization of nuisance signals including motion-derived parameters. Specifically, the first 10 volumes were excluded and the remaining data underwent slice-timing correction (AFNI 3dTshift). Then, the data were motion corrected using the first functional volume post-exclusion as the target image (AFNI 3dvolreg). Next, the data were smoothed (FWHM=2.5 mm), filtered (0.01–0.10 Hz), and effectively regressed of whole-brain, white matter (WM), cerebral spinal fluid (CSF), and six motion parameters corresponding to roll, pitch yaw, and displacement in the superior, left, and posterior directions (AFNI function: 3dBandpass). Note, the inclusion of motion vector orthogonalization was likely redundant given that the estimated motion in these anesthetized animals was negligible (e.g. the derivative of all motion parameters < 0.001). Within-animal alignment was performed via rigid body transformation of the functional data to the anatomical images (AFNI 3dAllineate). Between-animal alignment was performed by co-registering each animal's anatomical dataset to a separate template via a combination of linear (AFNI 3dAllineate) and non-linear (AFNI 3dQwarp) transformations. The result of each step in the pre-processing pipeline (tissue segmentation, alignment, etc.) was visually inspected for quality assurance.

Anatomical labeling

Brain structures of regions of interest in the 24 slices of the MR scans were determined using the relevant plates of a ferret brain atlas (included both histological and MRI structural sections of separate animals; plates of a ferret atlas provided by author Radtke-Schuller) as reference. Each *in vivo* MR slice (from the resting state data) was related to the corresponding atlas *in vivo* MRI image and histology section stained for cells (Nissl). The nomenclature of anatomical structures used is based on so far published data on the ferret and/or other carnivores (mainly cat and dog). Nissl stained sections of the brain atlas series (50 μm thick cryostat sections) referenced to the 24 MR slices of this study are shown with the relevant anatomical and functional labels.

Connectivity analysis

Following preprocessing, rsfMRI connectivity analyses were carried out using AFNI, FSL, and the Brain Connectivity Toolbox (Rubinov and Sporns, 2010). First, RSNs were produced using a data-driven gICA approach (FSL melodic). The number of independent components was set to 10. This number was chosen based on the observation that in humans, about 10 RSN can be consistently identified (Smith et al., 2009) and because we were using pre-processed data; thus we expected a smaller number of 'meaningful' components. The IC maps were thresholded (voxel-wise Z-score ≥ 1.96, i.e. two standard deviations) using an alternative hypothesis test based on fitting a Gaussian/gamma mixture model to the distribution of voxel intensities within spatial maps (Beckmann and Smith, 2004; Beckmann et al., 2005). The IC maps were then visually inspected and certain RSNs were selected for further analyses. RSNs were selected based on the following criteria, 1) consisted of relatively large continuous regions, 2) were

largely bilateral, and/or 3) could be referred to anatomical landmarks comparable to well-known structures in existing literature of ferrets and other mammals. For identification of brain regions within gICA connectivity maps, main foci were defined as regions that exhibited high connectivity strength (labeled in yellow) and satisfied the above criteria.

Ferret rsfMRI network connectivity properties were further analyzed using a graph theory approach. Graph measures (GMs) were computed using a graph representation of rsfMRI connectivity measures. Regions-of-interest (ROIs), representing the graph nodes, were defined within the pre-selected gICA networks (N=7). For each network, spherical ROIs (radius=1 mm, spatially non-overlapping) were defined as the top five local maxima (AFNI 3dExtrema, minimum distance=3 mm) resulting in a semi-dense (# of nodes=35) coverage of the brain. The minimum distance was based on a smoothness estimate from all animals ([X,Y,Z]= 2.80, 2.96, 2.20 mm; AFNI 3dFWHMx). The strength of connection between nodes was computed via temporal correlation analysis using each ROI as a seed region (AFNI 3dNetCorr). Fisher-Z transformed temporal correlation values, characterizing the connection strength between each pair of ROIs, were generated for each animal and then used to calculate various GMs. Within (average connectivity within a set of nodes) and between (average connectivity between sets of nodes) were compared across animals for each RSN. Within- and between-network connectivity was statistically validated across animals using standard *t*-tests. Significance was determined using a combined approach; $P < 0.05$ (uncorrected) and $\mu_{z\text{-Corr.}} \geq 0.1$. The small-world (SW) metric—a common brain network signature across species—was also computed. SW was computed using the clustering coefficient (CC; BCN Toolbox function) and characteristic path length (PL; BCN Toolbox function) and was determined by comparing the average CC and PL of the actual data (CC_A and PL_A) against random (CC_R and PL_R) permutations (BCN ToolBox function, n=1000 permutations);

$$SW=\left[CC_A/CC_R\right]/\left[PL_A/PL_R\right]$$

where values > 1 are indicative of a small world network. The SW parameter was calculated using thresholded (Z-correlation > 0.1) connectivity matrices. Distance measures (required for the PL measure) were computed as one minus the temporal correlation (i.e. high correlation values were represented by shorter distances). The ratio measures (log-transformed CC, PL, and SW) were also compared across animals using *t*-tests (h_0: $\log[X_A/X_R]=0$).

Results

Identification of resting state network (RSNs) in the ferret brain

We used gICA to derive RSNs in the ferret brain (Figs. 1–3). Preprocessed BOLD rsfMRI data collected from lightly anesthetized (0.5–0.75% isoflurane with xylazine, an anesthetic regimen studied in previous ferret studies (Sellers et al., 2013', 2015)) female ferrets (N=6) were used for the analysis. The components—or putative networks—were visually inspected and those not meeting our selection criteria (Fig. 3, N=3 networks) were excluded and the remaining networks (Figs. 1 and 2, N=7 networks) were further evaluated. These networks were topological consistent with RSNs observed in other species, and included the motor/somatosensory (#1 and #9), somatosensory (#2), auditory (#3), visual (#4) and putative default mode (DMN) (#5 [anterior] & #6 [posterior]) networks. The functional (bolded) and anatomical structures that exhibited high connectivity strengths (main foci) in each of these networks are listed as follows:

The main connectivity foci of the motor/somatosensory network (Fig. 1, IC[#1]) included **primary motor cortex** (M1) of the posterior sigmoid gyrus (PSG), **premotor cortex** (PM) of anterior sigmoid gyrus (ASG), **primary somatosensory cortex** (S1) in posterior sigmoid gyrus (PSG) and coronal gyrus (CNG), **higher order somatosensory cortex** namely the tertiary somatosensory area (S3) of suprasylvian gyrus (SSG) and caudate nucleus (NC) of the **basal ganglia**.

The second motor/somatosensory network (Fig. 1, IC[#9]) also included the main foci **primary motor cortex** (M1) in PSG, **premotor cortex** (PM) in ASG and **higher order somatosensory cortex** namely tertiary somatosensory area (S3) in lateral gyrus (LG), but the relative positions of these main foci were medial to that of IC[#1], and the primary somatosensory cortex and caudate nucleus were not included.

Main connectivity foci of the somatosensory network (Fig. 1, IC [#2]) included **primary somatosensory cortex** (S1) of PSG and CNG, **higher order somatosensory cortex** namely the tertiary somatosensory area (S3) of CNG, **multisensory cortex** in the medial bank of rostral suprasylvian sulcus (MRSS) of CNG, **rostral part of posterior parietal cortex** (PPr) of SSG and **functionally unidentified cortex** rostrally adjacent to S1 in PSG, pro-PSG and CNG.

Main connectivity foci of the auditory network (Fig. 1, IC[#3]) included **primary auditory cortex** (A1) in medial ectosylvian gyrus (MEG), **secondary and higher order auditory cortex** namely the anterior auditory field (AAF) in MEG, the posterior suprasylvian field (PSF) in posterior ectosylvian gyrus (PEG), the posterior pseudosylvian field (PPF) and pro-PPF (the rostral border region of PPF) of PEG, anterior ventral field (AVF) of the anterior ectosylvian gyrus (AEG), anterior dorsal field (ADF) of AEG, ventroposterior field (VP) in PEG, **multisensory cortex** in the medial bank of rostral suprasylvian sulcus (MRSS) of CNG, lateral bank of rostral suprasylvian sulcus (LRSS) of AEG, pseudosylvian sulcal cortex (PSSC) of AEG and PEG, **higher order visual cortex** in the anteromedial lateral suprasylvian cortex (AMLS) of SSG and anterolateral lateral suprasylvian cortex (ALLS) of MEG.

Main foci of the visual network (Fig. 1, IC[#4]) included primary visual cortex (area 17), **secondary and higher order visual cortex** namely area 18/19, area 21 of SSG, the anteromedial lateral suprasylvian cortex (AMLS) of SSG and anterolateral lateral suprasylvian cortex (ALLS) of MEG, the suprasylvian cortex (SSy), the **caudal part of posterior parietal cortex** (PPc) of SSG and LG, **postsplenial cortex** (PSC), **functionally undefined cortex** in rostral ventral PEG (vPEG) and NC of the **basal ganglia**.

We labeled the network #5 (Fig. 2A, IC[#5]) as a **putative anterior default mode network** as it was composed of main foci in **medial prefrontal cortex** namely prelimbic cortex (PL), medial **dorsal prefrontal cortex** (dPFC) in PRG and **premotor cortex** (PM) in ASG.

Additionally network #6 (Fig. 2B, IC[#6]) was deemed a **putative posterior default mode network** as it composed of main foci in **posterior parietal cortex** namely rostral posterior parietal cortex (PPr) in SSG and LG, caudal posterior parietal cortex (PPc) in SSG and LG, **posterior cingulate cortex** (CG), **higher order somatosensory cortex** tertiary somatosensory area (S3) in CNG, **multisensory cortex** of the medial bank of rostral suprasylvian sulcus (MRSS) in CNG and **primary motor cortex** (M1) in PSG.

Table 1 summarizes the location of each RSN in the corresponding anatomical regions in the ferret brain where main foci were defined as areas with strong correlation (labeled in yellow). All labeled brain areas spanned at least two consecutive slices.

Anatomical labeling of RSN brain regions

Main foci structures of high connectivity within networks were referenced to the relevant plates of a ferret brain histology atlas (ferret atlas provided by author Radtke-Schuller). The sections of the

histology atlas (Nissl-stained) were selected based on the corresponding *in vivo* atlas MR slices. Therefore, the structural template used for registering the resting state MR images was directly comparable to the sections of the atlas (Fig. 4). The nomenclature of anatomical structures used in the atlas was based on so far published data on the ferret and/or other carnivores. We used the references in the following paragraph to define brain regions within the gICA networks.

To localize the ferret's **somatosensory cortex** we used the following references for S1: Leclerc et al. (1993); Rice et al. (1993); McLaughlin et al. (1998); MRSS, LRSS: Keniston et al. (2009); S2,S3: Foxworthy and Meredith (2011); Meredith and Allman (2015); for **posterior parietal cortex** (PPr and PPc): Manger et al. (2002); Foxworthy and Meredith (2011); Foxworthy et al. (2013b); for **visual cortex** area 17: Rockland (1985); Henderson (1987); Law et al. (1988); Innocenti et al. (2002) (also for areas 18, 19 and 21); area 20 (20a, 20b): Manger et al. (2004); SSy and other areas: Cantone et al. (2005). The region of SSy has been renamed by several authors, for example see Homman-Ludiye et al. (2010). For AMLS, ALLS we used Manger et al. (2008); for **auditory cortex** (primary and higher order cortex) we used Bizley et al. (2005); Bajo et al. (2007); Atiani et al. (2014); for PSSC we used Ramsay and Meredith (2004). For **frontal cortex** (dPFC, PM and CG; also for primary motor cortex) we referenced Mustela and Cercoleptes (Brodmann, 1909), dog (Kreiner, 1961), ferret PFC (Duque and McCormick, 2010; Fritz et al., 2010) studies; for PL (cat) (Room et al., 1985). For **RSG** and **PSC** we referred to the cat (Olson and Musil, 1992).

Quantification of within- and between-network connectivity

We noticed two interesting features in our dataset: first, gICA analysis revealed two separate components embodying the anterior and posterior DMNs. Previous studies have shown that the DMN is composed of dissociate, yet interconnected subnetworks (Andrews-Hanna et al., 2010; Lu et al., 2012; Kyathanahally et al., 2015). Second, we found an abundance of motor and somatosensory related gICA components, which seemed to be unique to our dataset. To shed light on these two features and to further quantify the connectivity patterns present within our dataset, we computed within- and between-network connectivity using correlation analysis. The ferret brain was subdivided into a set of non-overlapping nodes or regions-of-interest (ROIs, Fig. 5A) using the included RSNs detailed above (Fig. 1: IC's #1-4 & #9, and Fig. 2; IC's #5 & #6]). Temporal correlation was used to define the strength of connection between

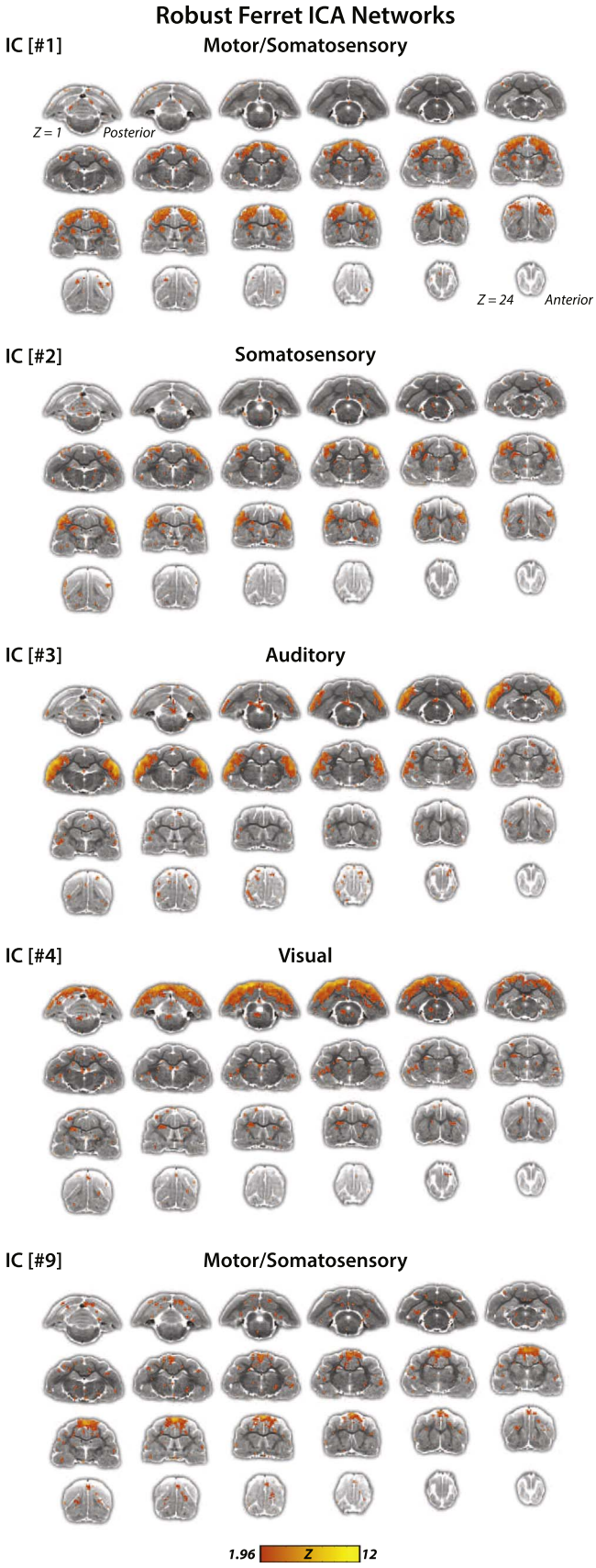

Fig. 1. Ferret gICA networks. IC[#1] Motor/somatosensory network identified from the gICA analysis. Connectivity maps included **primary motor cortex** (M1 located on the PSG), **premotor cortex** (PM on ASG), **primary somatosensory cortex** (S1 on PSG and CNG), **higher order somatosensory cortex** (**tertiary somatosensory area** (S3 on SSG), and **basal ganglia** (caudate nucleus (NC)). Connectivity maps are overlaid onto T2-anatomical images with red-yellow color encoding using a $1.96 < Z\text{-score} < 12$ threshold (see colorbar); same conventions for ICs #2-4. IC[#2] Somatosensory network identified from the gICA analysis. Connectivity maps included the brain regions **primary somatosensory cortex** (S1 on PSG and CNG), **multisensory cortex** (MRSS on medial bank of rostral suprasylvian sulcus), **posterior parietal cortex** (PPr on SSG) and **higher order somatosensory cortex** (tertiary somatosensory area (S3 on SSG), and **functionally unidentified cortex** rostrally adjacent to S1 (on PSG, pro-PSG, and CNG). IC[#3] Auditory network identified from the gICA analysis. Connectivity maps included all **primary and higher order auditory cortex fields**, and **adjacent multisensory and higher order visual cortex fields** (summarized, see List 1 for all included regions). IC[#4] Visual network identified from the gICA analysis. Connectivity maps included the brain regions **primary visual cortex** (area 17), **secondary and higher order visual cortex** (area 18/19 on LG; area 21 on SSG; ALMS on SSG; ALLS on MEG; suprasylvian cortex (SSy), **posterior parietal cortex** (PPc on SSG and LG), **postsplenial cortex** (PSC), **functionally undefined cortex** (presumed higher order auditory cortex on vPEG) and **basal ganglia** (caudate nucleus (NC)). IC[#9] Motor/somatosensory network identified from the gICA analysis. Connectivity maps included the brain regions **primary motor cortex** (M1 on PSG), **premotor cortex** (PM on ASG), and **higher order somatosensory cortex** (tertiary somatosensory area (S3 on LG). (For interpretation of the references to color in this figure legend, the reader is referred to the web version of this article.)

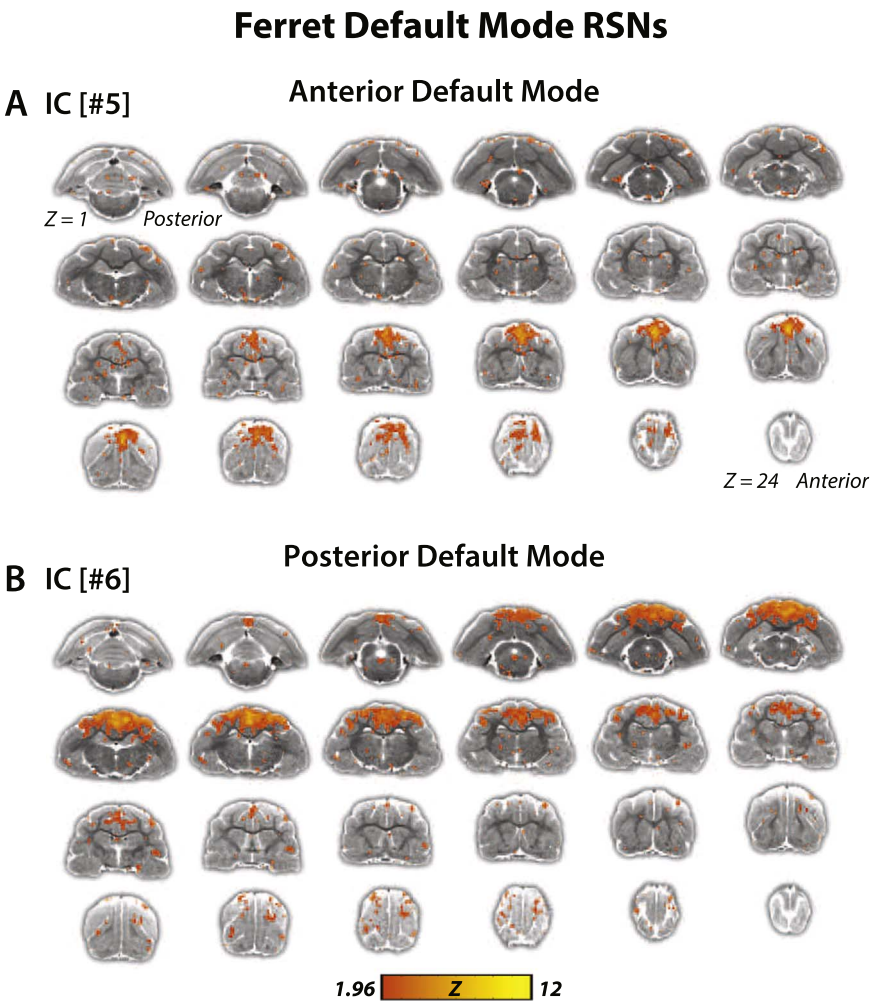

Fig. 2. Anterior and posterior default mode networks of the ferret brain. (A). Putative anterior default mode network (IC[#5]) identified from the gICA analysis. Connectivity maps included the brain regions medial PFC, medial dPFC, and PM. Connectivity maps are overlaid onto T2-anatomical images with red-yellow color encoding using a $1.96 < \text{Z-score} < 12$ threshold (see colorbar). (B). Putative posterior default mode network (IC[#6]) identified from the gICA analysis. Connectivity maps included the brain regions posterior parietal cortex, posterior cingulate cortex, S3, MRSS and M1. (For interpretation of the references to color in this figure legend, the reader is referred to the web version of this article.)

nodes and the total pair-wise representation, or correlation matrix, was used to compute graph measures. The mean Fisher's-Z transformed correlation matrix (Fig. 5B) was typified by strong within network connectivity (main diagonal) and moderate between network connectivity. Within and between RSN connectivity was quantified using the average correlation measures for each set of nodes (Fig. 5C within-white and between-grey). All RSNs had significant (Fig. 5C; * represents $P < 0.05$ uncorrected, $\mu_{\text{Z-Correlation}} \geq 0.10$) within-network connectivity. Significant between-network connectivity was also detected for a subset of networks including somatosensory/motor (IC #1 and #2; $P=0.011$), anterior DMN and posterior DMN (IC #5 and #6; $P=0.015$), and motor with both anterior DMN (IC #9 and #5; $P=0.014$) and posterior DMN (IC #9 and #6; $P=0.012$).

Graph measures confirm "small-world" brain network topology in ferrets

The human brain exhibits network properties that are characterized by optimal spatial and metabolic efficiency for global and local parallel information processing (Bullmore and Sporns, 2012; Uehara et al., 2014). To determine if the ferret brain also displays this economic network organization, we used graph theory to quantify the efficiency of ferret brain connectivity. Overall brain network architecture was assessed in each animal using the "small-world" (SW) graph measure (Table 2), a metric based on the clustering coefficient (CC) and characteristic path length (PL) of the actual data versus random simulations (see methods for full details). Small-world networks ($SW > 1$) are characterized by a short overall PL and a high CC. The PL was similar between the actual and random data however the CC was statistically different ($P=0.002$) resulting in an average SW significantly greater than 1 ($P=0.003$). Taken together, these results indicate that the functional connectivity patterns within and between networks in the ferret brain are optimized for efficient local and long-range communication.

Discussion

Due to the ability to acquire data from both animals and humans in the same manner, rsfMRI has emerged as a powerful translational method for bridging preclinical and human studies. In conjunction with data-driven gICA and graph theory analysis methods, rsfMRI has proven to be a robust approach to identify and characterize similar brain networks across species. Here we report the presence of seven networks (two motor/somatosensory, somatosensory, auditory, visual, anterior DMN, and posterior DMN) in the ferret brain similar to those previously shown in

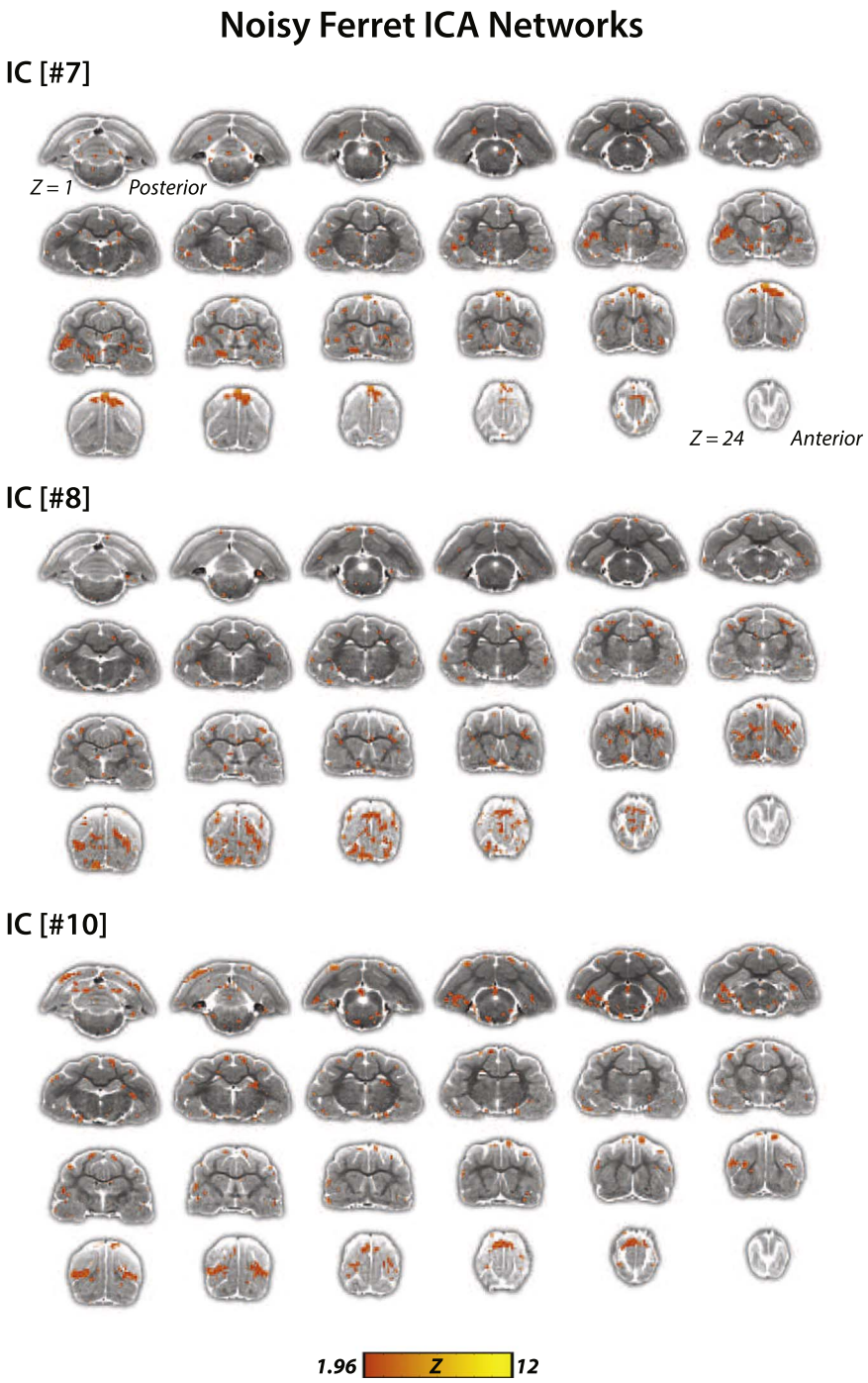

Fig. 3. Excluded gICA Networks. Group-level ICA components #7, 8, and 10 were excluded from further analysis upon failing the following criteria, components 1) consisted of relatively large continuous regions with Z-Correlations > 1.96, 2) connectivity patterns were largely bilateral, and/or 3) could be referred to anatomical landmarks comparable to well-known structures in existing literature of ferrets and other mammals. Connectivity maps are overlaid onto T2-anatomical images with red-yellow color encoding using a 1.96 < Z-score < 12 threshold (see colorbar). (For interpretation of the references to color in this figure legend, the reader is referred to the web version of this article.)

human and animal data (Damoiseaux et al., 2006; Vincent et al., 2007; Lu et al., 2012; Belcher et al., 2013; Mechling et al., 2014; Stafford et al., 2014; Kyathanahally et al., 2015). We found interconnected motor and somatosensory networks, and interconnected DMN sub-networks using correlation analyses. We further explored the network topology using graph theory analysis and found that the ferret brain is economically organized in a small-world manner. Together, our data supports the presence of modular and stereotyped resting state networks, including a DMN, conserved across species. Further, these results argue for the study of the ferret as an animal model for translational research, and provide a foundation for future ferret brain mapping.

Comparison to human and animal resting state literature

Previous resting state functional connectivity studies have reported a breadth of canonical resting state networks stable across species and sessions. Consistent with existing studies, we observed

the presence of multiple sensory and motor networks (Damoiseaux et al., 2006; Lu et al., 2012; Belcher et al., 2013). Fractionation of sensory and motor networks is observed in human and non-human primate literature (Damoiseaux et al., 2006; Belcher et al., 2013), perhaps indicative of distinct primary and higher-order networks. We found several somatosensory and motor networks similar to studies in mice, rats, and non-human primates (Hutchison et al., 2010; Belcher et al., 2013; Mechling et al., 2014; Gozzi and Schwarz, 2016); however, we found a single network for the visual regions, contrasting the primary and higher-order separations seen in the aforementioned studies. This may be explained by the limited coverage of V1 in our scans (due to constrained field of view parameters), or that the ferret visual system is integrated in its functional connectivity. The fractionation of sensory areas may arise from a structural basis: for example, S1, S2, and S3 of rats, ferrets, monkeys receive inputs from distinct regions of thalamus (Friedman and Murray, 1986; Spreafico et al., 1987; Foxworthy and Meredith, 2011). Thalamic subdivisions encode and relay unique information (Marlinski and McCrea, 2008), and may synchronize with cortical subregions in different communication channels (ie. functional networks).

The DMN, which has been extensively characterized in several other animals and the human, is of particular interest due to its involvement in states of self-reference and rest and its relevance to mental disorders (Raichle and Snyder, 2007; Buckner et al., 2008; Raichle, 2015). Human and non-human primate studies consistently show that the DMN is comprised of the medial PFC, posterior cingulate cortex (PCC), inferior parietal cortex, lateral temporal cortex, and the hippocampus (Damoiseaux et al., 2006; Buckner et al., 2008). Similar connectivity patterns have been observed in animal studies with medial PFC and PCC showing up the most consistently in the reported DMNs (Vincent et al., 2007; Andrews-Hanna et al., 2010; Lu et al., 2012). We found in the ferret a putative anterior DMN that included the medial and dorsal PFC, and a posterior DMN that included the posterior cingulate and posterior parietal cortex. Key differences between the ferret and rodent DMNs lie in the presence of the orbitofrontal cortex and hippocampus (Lu et al., 2012; Sforazzini et al., 2014; Zerbi et al., 2015). The orbitofrontal cortex is present in the DMN of both rodents but not the ferret, and the hippocampus is present in the rat, but not the ferret and mouse. The absence of orbitofrontal cortex in the ferret DMN may not be a surprising observation as it seems to form its own network in higher order animals (Belcher et al., 2013), and occupies a functional role in reward-related behavior rather than rest and quiescence (Kringelbach, 2005). Despite these differences, our results overall support the presence of defined and consistent resting state networks, invariant of animal species.

While there is evidence that anesthesia alters the dynamic properties of functional connectivity (Barttfeld et al., 2015; Liang et al., 2015), resting state networks persist during anesthesia, albeit slightly diminished in connectivity magnitude (Vincent et al., 2007; Hutchison et al., 2013). Signatures of functional networks in awake states, such as anatomically-confined and bilateral

Table 1
Main anatomical regions labeled in gICA maps. Anatomical regions that were labeled in the gICA connectivity maps are listed for each network. These main foci structures were defined by areas with strong correlation (Z-scores labeled in yellow in the gICA maps). All labeled brain areas spanned at least two consecutive slices. Additional conventions and criteria for anatomical labeling can be found in the methods. See List 1 for anatomical abbreviations.

Network #	Main anatomical regions included in gICA networks
Network 1	M1, PM, S1, S3, NC
Network 2	S1, MRSS, PPr, S3
Network 3	A1, AAF, PPF/proPPF, PSF, AVF, ADF, PSSC, VP, MRSS, LRSS, AMLS, ALLS
Network 4	Area 17, Area 18/19, Area, 21, PPc, SSy, AMLS, ALLS, PSC, vPEG, NC
Network 5	mPFC (PL), dPFC, PM
Network 6	PPr, PPc, CG, S3, MRSS, M1
Network 9	M1, PM, S3

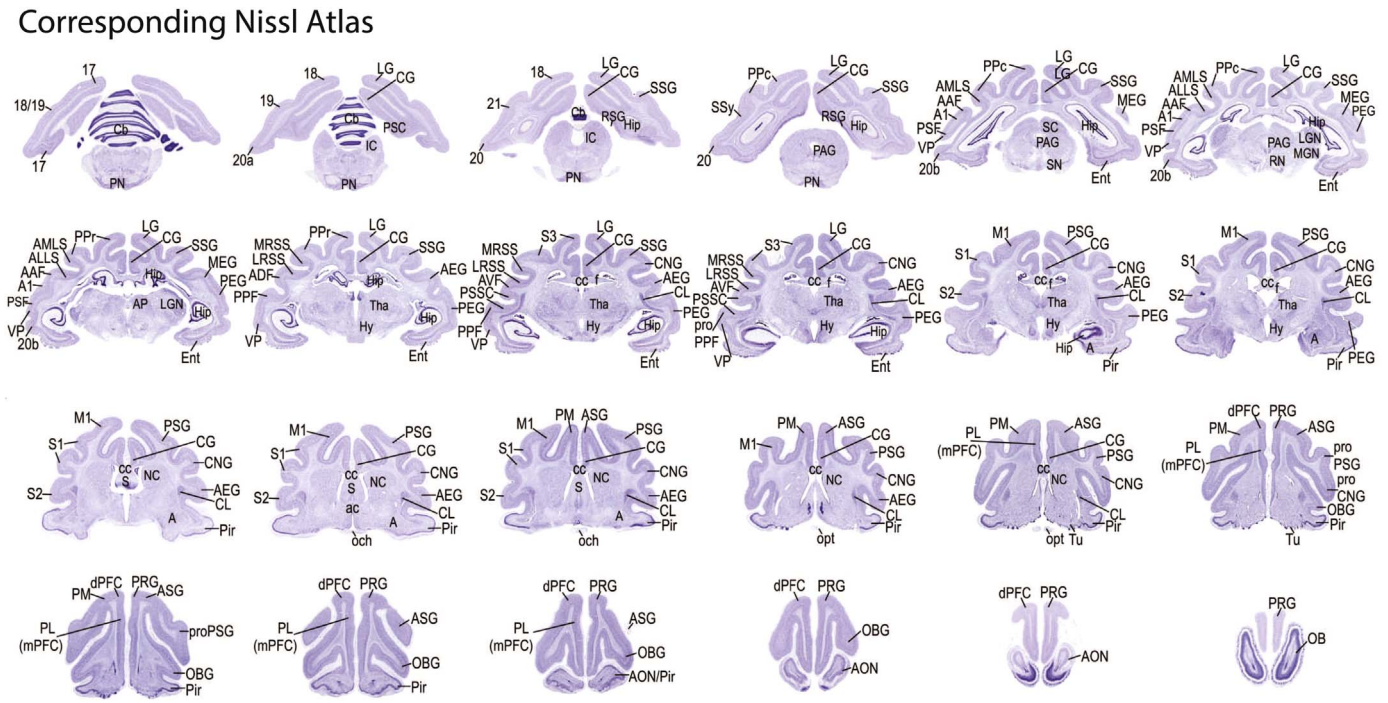

Fig. 4. Nissl stain sections corresponding to MRI slices. Nissl stained sections of the ferret brain atlas (50 μm thick cryostat sections; ferret atlas provided by author Radtke-Schuller) corresponding to the MR images from this study are shown with relevant anatomical and functional labels for the main foci found in the gICA maps and further anatomical labels for orientation. The labeling of anatomical structures used in this atlas was based on currently published data on the ferret and/or other carnivores (mainly cat and dog). Functional and structural nomenclatures are indicated on the left and right hemisphere, respectively.

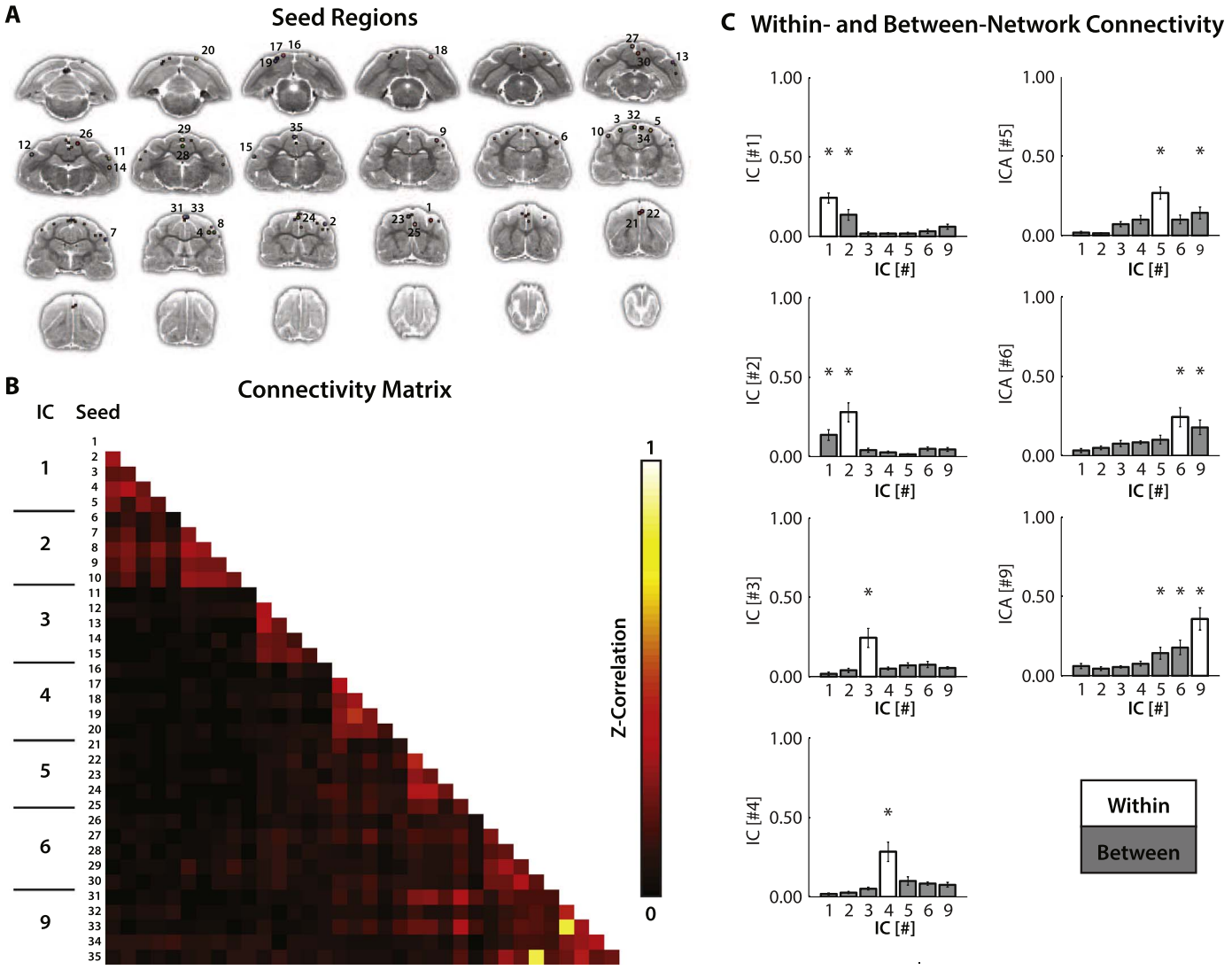

Fig. 5. Within- and between-network connectivity analysis. (A). Seeds for connectivity analysis. To compute within- and between-network connectivity, five spherical (radius of 1 mm) regions-of-interest (ROIs) were identified for each network. These ROIs were centered at the top five local maxima of the correlation map (minimum distance between each maxima was 3 mm), and served as representative samples of each network. Average BOLD time-series were extracted from each of the ROIs for subsequent correlation analysis. (B). Mean connectivity matrix. Group-level connectivity matrix of the average pair-wise correlations between the generated ROIs. Cells along the diagonal represent within-network connections and those that are off the diagonal represent between-network connections. Z-correlation strengths from 0 to 1 are represented by colors ranging from black to red to white (see colorbar). (C). Quantification of within- and between-network connectivity. To quantify the degree of within- and between-network connectivity, ROI correlation values were averaged across pairs for each network. Each bar graph represents mean correlation values relative to a particular network. White bars signify average correlation values for ROI pairs within the network and gray bars signify average correlation values for pairs where native ROIs were connected to ROIs in outside networks. $^{*}P < 0.05$ *(uncorrected) and* $\mu_{Z\text{-}Corr.} \geq 0.1$. (For interpretation of the references to color in this figure legend, the reader is referred to the web version of this article.)

connectivity patterns, remain prominent under low levels of isoflurane anesthesia (Grandjean et al., 2014). Nevertheless, the use of anesthesia is a potential confound and limitation for our study (Sellers et al., 2013, 2015).

The functionally connected brain regions that comprised the gICA network maps ultimately depend on the analysis method and the level of thresholding applied to the dataset (Hutchison et al., 2013). We opted for a conservative approach to identify brain regions that contribute to the gICA networks. Brain regions were defined by areas in the gICA connectivity map that passed the criteria of 1) Z-Correlations > 1.96, 2) strong, contiguous correlation values, and 3) labels spanning at least two consecutive slices. Using these criteria, we identified functional network maps that were both anatomically relevant and stringently defined.

Significance of the ferret DMN

Several studies have reported that the DMN exhibits modular organization; in other words, the DMN is composed of sub-networks centered on key hubs. Comparative anatomy in monkeys and humans suggests that the medial PFC and PCC serve as hubs due to their rich connectivity patterns with other association areas that are also present in the DMN (Buckner et al., 2008). Indeed, we found two distinct interconnected networks that contained the PFC and PCC, suggesting that ferrets possess a subset of resting state networks that resemble the DMN in higher-order animals.

Lu and colleagues highlighted that the rat DMN runs along the length of the midline from medial PFC to the PCC, as opposed to a focal localization in the monkey (Lu et al., 2012). Taking into account the motor sub-network connected with the DMN, we

Table 2
Consistent small-world network properties across animals. The small-world (SW) metric was calculated as a ratio of the relative clustering coefficient (CC) to the relative characteristic path length (PL). Relative CC and PL were calculated as a ratio of the average values from the actual data (A) to that of randomly generated permutations (R). As small-world networks exhibit higher local clustering and similar path lengths compared to random networks, we would expect $CC > 1$ and $PL = 1$. A SW value significantly greater than 1 indicates that the network exhibited small-world properties. μ = mean, SE = Standard Error.

Animal	CC_A	CC_R	$\frac{CC_A}{CC_R}$	PL_A	PL_R	$\frac{PL_A}{PL_R}$	$SW\ \frac{[CC_A/CC_R]}{[PL_A/PL_R]}$
1	0.123	0.101	1.221	0.853	0.841	1.013	1.206
2	0.063	0.049	1.281	0.891	0.888	1.003	1.277
3	0.094	0.069	1.365	0.889	0.887	1.002	1.362
4	0.055	0.047	1.161	0.912	0.912	1.000	1.161
5	0.129	0.106	1.213	0.843	0.825	1.021	1.187
6	0.120	0.075	1.596	0.884	0.881	1.004	1.590
μ	0.097	0.075	1.306	0.879	0.872	1.007	1.297
SE	0.013	0.010	0.065	0.011	0.013	0.003	0.066

observed a similar pattern of posterior to anterior spread. Cat PCC receives input from higher-order sensory and premotor areas (Olson and Musil, 1992), and is active during visually-guided eye movements (Olson and Musil, 1992; Vogt and Gabriel, 1993). Given that cats and ferrets are both in the order Carnivora, it may be possible that PCC of both species share similarities in connectivity, explaining the inclusion of the midline motor regions in ferret DMN. The conclusions we are able to draw regarding the relationship between structural and functional connectivity are restricted by the limited number of ferret brain anatomical, and especially connectivity, studies. Future work may address this gap in the literature using diffusion tensor imaging and tract tracing.

While the functional relevance of the DMN in animals is debated, some studies shed light on how such a network could be important in animal behavior. One study showed that the homologous DMN in chimpanzees is most active at rest, moderately active during social tasks, and minimally active during non-social tasks (Barks et al., 2015). Additionally, the DMN sub-network centered on the posterior cingulate and mPFC is active during self-relevant affective cognition (Andrews-Hanna et al., 2010). Social behavior is evolutionarily conserved across animals and is beneficial to species survival. It may be possible that collective DMN brain activity relates to social, affective cognition known to be present in rodents, non-human primates, and potentially ferrets (Poole, 1978; Trezza et al., 2011; Gunaydin et al., 2014; Harris, 2015). Given these previous findings, the DMN poses as a prime target for the study of brain pathologies and impairments in these functional domains. Although our study lacked targeted manipulation of the resting state networks, such perturbation would be the logical progression for future translational studies.

Small-world network properties of the ferret brain

This modular organization of the DMN and, more broadly, complex networks subserves efficiency and optimization of information transfer across brain regions. Highly complex natural networks that require a balance between metabolic cost and information processing capacity exhibit a large degree of local clustering and few random, long-range connections (Watts and Strogatz, 1998; Achard et al., 2006; Bullmore and Sporns, 2012). Such organization facilitates specialization within local nodes, as well as efficient parallel processing of distributed sub-networks. Several studies have utilized graph theory metrics, such as small-world and rich-club properties, to show that human and animal brain networks exhibit pronounced local clustering with sparse long-range connections (Hosseini and Kesler, 2013; Baliki et al., 2014; Collin et al., 2014; Miranda-Dominguez et al., 2014). We used the small-world graph theory metric to similarly measure how efficiently the ferret brain is connected. We found that, consistent across all recorded animals, the ferret brain network exhibits small world properties of high clustering coefficients. The characteristic path length was longer than expected of a small world network; however, recent studies have shown that path length increases with loss of consciousness (Monti et al., 2013; Uehara et al., 2014). As a whole, these data concur with previous reports of small-world characteristics of human and animal resting state networks. Our results add to the growing evidence that optimal brain metabolism and information processing benefit from highly-connected, specialized local nodes and distributed long-range wiring patterns.

Importance of ferret brain research

Systems neuroscience has experienced a dramatic shift away from using a broad set of model species towards the almost exclusive use of mice due to the availability of genetic tools. More recent developments in the realm of genetic engineering are now enabling a reconsideration of model species beyond the mouse. As a result, the interest in intermediate model species such as the ferret is undergoing a resurgence. For example, recent research has made considerable headway in mapping distinct anatomical and functional regions of the ferret brain. In particular, the function of the ferret visual and auditory cortices has been well characterized (Basole et al., 2003; Li et al., 2008; Bizley and King, 2009; Bizley et al., 2015; Smith et al., 2015; Town et al., 2015; Roy et al., 2016). There is substantial evidence for the sophistication of the ferret visual system through development. Specifically, the development of motion and orientation selectivity in the ferret visual cortex depends on propagating population activity dynamics within stimulus-selective columns (Li et al., 2008; Smith et al., 2015). These stimulus-property-selective dominance columns, present in cats, non-human primates, and humans, may play an expanded role in downstream visual information processing. Studies in the ferret auditory cortex have highlighted similarities between ferret and human uni-modal and multi-modal auditory processing (Bizley et al., 2012; Atiani et al., 2014; Town et al., 2015). As many neuropsychiatric disorders involve multi-modal impairments in sensory processing, the dissection of mechanisms underlying such facilities is particularly important. Additionally, recent efforts have been made to establish the role of frontal cortex regions in sensory regulation (Fritz et al., 2010; Zhou et al., 2016b). Ferret frontal cortex provides top-down sensory gating and stimulus selection in both auditory and visual conditions, reminiscent of the regulatory role of prefrontal cortex in monkeys and humans (Fuster, 2015). Results in our study provide functional validation for the inter-areal connections (overlapping sensory regions in networks 3 and 4) important for cross-modal cognitive processing, and may serve as a foundation for exploring new circuits involved in such processes.

Conclusion

In summary, we assessed whether the resting ferret brain exhibits distinct, functionally connected networks similar to those reported in humans and non-human primates. Indeed, we provided evidence for the presence of multiple, consistent sensory, motor, and higher-order networks in the ferret brain. Importantly, these results support the notion that resting state functional networks are conserved across species, and reflect the optimized brain architecture that subserves demanding cognitive computations. Our data provide a foundation for modeling psychiatric disorders through perturbation of intrinsic connectivity, and

ultimately, the assessment of the mechanisms underlying these disorders.

Authorship statement

ZZ, YIS, and FF designed the experiments, ZZ, YL, and KKS performed the experiments, AS and WG analyzed the data, SRS performed histology and labeling, and ZZ, AS, SRS, WG, FF, and JHG wrote the paper.

The authors declare no competing financial interests.

Acknowledgments

The authors would like to thank present and past members of the Fröhlich Lab for their support. The authors would like to acknowledge the UNC Small Animal Imaging Facility for their aid during data acquisition. The authors gratefully acknowledge the funding sources; the work was in part funded by UNC Department of Psychiatry, the Human Frontier Science Program (Project ID RGY0068/2014), and by the National Institute of Mental Health of the National Institutes of Health under Award no. R01MH101547, and the Cedars-Sinai Institutional Support to WG. The content is solely the responsibility of the authors and does not necessarily represent the official views of the National Institutes of Health.

References

Achard, S., Salvador, R., Whitcher, B., Suckling, J., Bullmore, E., 2006. A resilient, low-frequency, small-world human brain functional network with highly connected association cortical hubs. J. Neurosci. 26, 63–72.
Andrews-Hanna, J.R., Reidler, J.S., Sepulcre, J., Poulin, R., Buckner, R.L., 2010. Functional-anatomic fractionation of the brain's default network. Neuron 65, 550–562.
Atiani, S., David, S.V., Elgueda, D., Locastro, M., Radtke-Schuller, S., Shamma, S.A., Fritz, J.B., 2014. Emergent selectivity for task-relevant stimuli in higher-order auditory cortex. Neuron 82, 486–499.
Bajo, V.M., Nodal, F.R., Bizley, J.K., Moore, D.R., King, A.J., 2007. The ferret auditory cortex: descending projections to the inferior colliculus. Cereb. Cortex 17, 475–491.
Baliki, M.N., Chang, P.C., Baria, A.T., Centeno, M.V., Apkarian, A.V., 2014. Resting-sate functional reorganization of the rat limbic system following neuropathic injury. Sci. Rep. 4, 6186.
Barks, S.K., Parr, L.A., Rilling, J.K., 2015. The default mode network in chimpanzees (Pan troglodytes) is similar to that of humans. Cereb. Cortex 25, 538–544.
Barnette, A.R., Neil, J.J., Kroenke, C.D., Griffith, J.L., Epstein, A.A., Bayly, P.V., Knutsen, A.K., Inder, T.E., 2009. Characterization of brain development in the ferret via MRI. Pediatr. Res. 66, 80–84.
Barttfeld, P., Uhrig, L., Sitt, J.D., Sigman, M., Jarraya, B., Dehaene, S., 2015. Signature of consciousness in the dynamics of resting-state brain activity. Proc. Natl. Acad. Sci. USA 112, 887–892.
Basole, A., White, L.E., Fitzpatrick, D., 2003. Mapping multiple features in the population response of visual cortex. Nature 423, 986–990.
Beckmann, C.F., Smith, S.M., 2004. Probabilistic independent component analysis for functional magnetic resonance imaging. IEEE Trans. Med. Imaging 23, 137–152.
Beckmann, C.F., DeLuca, M., Devlin, J.T., Smith, S.M., 2005. Investigations into resting-state connectivity using independent component analysis. Philos. Trans. R. Soc. Lond. B Biol. Sci. 360, 1001–1013.
Belcher, A.M., Yen, C.C., Stepp, H., Gu, H., Lu, H., Yang, Y., Silva, A.C., Stein, E.A., 2013. Large-scale brain networks in the awake, truly resting marmoset monkey. J. Neurosci. 33, 16796–16804.
Biswal, B., Yetkin, F.Z., Haughton, V.M., Hyde, J.S., 1995. Functional connectivity in the motor cortex of resting human brain using echo-planar MRI. Magn. Reson. Med. 34, 537–541.
Bizley, J.K., King, A.J., 2009. Visual influences on ferret auditory cortex. Hear Res. 258, 55–63.
Bizley, J.K., Shinn-Cunningham, B.G., Lee, A.K., 2012. Nothing is irrelevant in a noisy world: sensory illusions reveal obligatory within-and across-modality integration. J. Neurosci. 32, 13402–13410.
Bizley, J.K., Nodal, F.R., Nelken, I., King, A.J., 2005. Functional organization of ferret auditory cortex. Cereb. Cortex 15, 1637–1653.
Bizley, J.K., Bajo, V.M., Nodal, F.R., King, A.J., 2015. Cortico-cortical connectivity within ferret auditory cortex. J. Comp. Neurol. 523, 2187–2210.
Brodmann, K., 1909. Vergleichende Lokalisationslehre der Grosshirnrinde. Johann Ambrosius Barth, Leipzig.
Brusa, L., Ponzo, V., Mastropasqua, C., Picazio, S., Bonni, S., Di Lorenzo, F., Iani, C., Stefani, A., Stanzione, P., Caltagirone, C., Bozzali, M., Koch, G., 2014. Theta burst stimulation modulates cerebellar-cortical connectivity in patients with progressive supranuclear palsy. Brain Stimul. 7, 29–35.
Buckner, R.L., Andrews-Hanna, J.R., Schacter, D.L., 2008. The brain's default network: anatomy, function, and relevance to disease. Ann. NY Acad. Sci. 1124, 1–38.
Bullmore, E., Sporns, O., 2012. The economy of brain network organization. Nat. Rev. Neurosci. 13, 336–349.
Cantone, G., Xiao, J., McFarlane, N., Levitt, J.B., 2005. Feedback connections to ferret striate cortex: direct evidence for visuotopic convergence of feedback inputs. J. Comp. Neurol. 487, 312–331.
Collin, G., Sporns, O., Mandl, R.C., van den Heuvel, M.P., 2014. Structural and functional aspects relating to cost and benefit of rich club organization in the human cerebral cortex. Cereb. Cortex 24, 2258–2267.
Damoiseaux, J.S., Rombouts, S.A., Barkhof, F., Scheltens, P., Stam, C.J., Smith, S.M., Beckmann, C.F., 2006. Consistent resting-state networks across healthy subjects. Proc. Natl. Acad. Sci. USA 103, 13848–13853.
Duque, A., McCormick, D.A., 2010. Circuit-based localization of ferret prefrontal cortex. Cereb. Cortex 20, 1020–1036.
Empie, K., Rangarajan, V., Juul, S.E., 2015. Is the ferret a suitable species for studying perinatal brain injury? Int. J. Dev. Neurosci. 45, 2–10.
Fox, M.D., Buckner, R.L., White, M.P., Greicius, M.D., Pascual-Leone, A., 2012. Efficacy of transcranial magnetic stimulation targets for depression is related to intrinsic functional connectivity with the subgenual cingulate. Biol. Psychiatry 72, 595–603.
Foxworthy, W.A., Meredith, M.A., 2011. An examination of somatosensory area SIII in ferret cortex. Somatosens. Mot. Res. 28, 1–10.
Foxworthy, W.A., Clemo, H.R., Meredith, M.A., 2013a. Laminar and connectional organization of a multisensory cortex. J. Comp. Neurol. 521, 1867–1890.
Foxworthy, W.A., Allman, B.L., Keniston, L.P., Meredith, M.A., 2013b. Multisensory and unisensory neurons in ferret parietal cortex exhibit distinct functional properties. Eur. J. Neurosci. 37, 910–923.
Friedman, D.P., Murray, E.A., 1986. Thalamic connectivity of the second somatosensory area and neighboring somatosensory fields of the lateral sulcus of the macaque. J. Comp. Neurol. 252, 348–373.
Fritz, J.B., David, S.V., Radtke-Schuller, S., Yin, P., Shamma, S.A., 2010. Adaptive, behaviorally gated, persistent encoding of task-relevant auditory information in ferret frontal cortex. Nat. Neurosci. 13, 1011–1019.
Fuster, J., 2015. The Prefontal Cortex. Elsevier, Boston, MA.
Gozzi, A., Schwarz, A.J., 2016. Large-scale functional connectivity networks in the rodent brain. Neuroimage 127, 496–509.
Grandjean, J., Schroeter, A., Batata, I., Rudin, M., 2014. Optimization of anesthesia protocol for resting-state fMRI in mice based on differential effects of anesthetics on functional connectivity patterns. Neuroimage 102 (Pt 2), 838–847.
Greicius, M.D., Srivastava, G., Reiss, A.L., Menon, V., 2004. Default-mode network activity distinguishes Alzheimer's disease from healthy aging: evidence from functional MRI. Proc. Natl. Acad. Sci. USA 101, 4637–4642.
Greicius, M.D., Supekar, K., Menon, V., Dougherty, R.F., 2009. Resting-state functional connectivity reflects structural connectivity in the default mode network. Cereb. Cortex 19, 72–78.
Gunaydin, L.A., Grosenick, L., Finkelstein, J.C., Kauvar, I.V., Fenno, L.E., Adhikari, A., Lammel, S., Mirzabekov, J.J., Airan, R.D., Zalocusky, K.A., Tye, K.M., Anikeeva, P., Malenka, R.C., Deisseroth, K., 2014. Natural neural projection dynamics underlying social behavior. Cell 157, 1535–1551.
Harris, L.M., 2015. Ferret wellness management and environmental enrichment. Vet. Clin. North Am. Exot. Anim. Pract. 18, 233–244.
Henderson, Z., 1987. Cholinergic innervation of ferret visual system. Neuroscience 20, 503–518.
Homman-Ludiye, J., Manger, P.R., Bourne, J.A., 2010. Immunohistochemical parcellation of the ferret (Mustela putorius) visual cortex reveals substantial homology with the cat (Felis catus). J. Comp. Neurol. 518, 4439–4462.
Hosseini, S.M., Kesler, S.R., 2013. Comparing connectivity pattern and small-world organization between structural correlation and resting-state networks in healthy adults. Neuroimage 78, 402–414.
Hutchison, R.M., Mirsattari, S.M., Jones, C.K., Gati, J.S., Leung, L.S., 2010. Functional networks in the anesthetized rat brain revealed by independent component analysis of resting-state FMRI. J. Neurophysiol. 103, 3398–3406.
Hutchison, R.M., Womelsdorf, T., Gati, J.S., Everling, S., Menon, R.S., 2013. Resting-state networks show dynamic functional connectivity in awake humans and anesthetized macaques. Hum. Brain Mapp. 34, 2154–2177.
Innocenti, G.M., Manger, P.R., Masiello, I., Colin, I., Tettoni, L., 2002. Architecture and callosal connections of visual areas 17, 18, 19 and 21 in the ferret (Mustela putorius). Cereb. Cortex 12, 411–422.
Karbasforoushan, H., Woodward, N.D., 2012. Resting-state networks in schizophrenia. Curr. Top. Med. Chem. 12, 2404–2414.
Keniston, L.P., Allman, B.L., Meredith, M.A., Clemo, H.R., 2009. Somatosensory and multisensory properties of the medial bank of the ferret rostral suprasylvian sulcus. Exp. Brain Res. 196, 239–251.
Kou, Z., Wu, Q., Kou, X., Yin, C., Wang, H., Zuo, Z., Zhuo, Y., Chen, A., Gao, S., Wang, X., 2015. CRISPR/Cas9-mediated genome engineering of the ferret. Cell Res. 25, 1372–1375.
Kreiner, J., 1961. The myeloarchitectonics of the frontal cortex of the dog. J. Comp. Neurol. 116, 117–133.

Kringelbach, M.L., 2005. The human orbitofrontal cortex: linking reward to hedonic experience. Nat. Rev. Neurosci. 6, 691–702.
Kyathanahally, S.P., Jia, H., Pustovyy, O.M., Waggoner, P., Beyers, R., Schumacher, J., Barrett, J., Morrison, E.E., Salibi, N., Denney, T.S., Vodyanoy, V.J., Deshpande, G., 2015. Anterior-posterior dissociation of the default mode network in dogs. Brain Struct. Funct. 220, 1063–1076.
Law, M.I., Zahs, K.R., Stryker, M.P., 1988. Organization of primary visual cortex (area 17) in the ferret. J. Comp. Neurol. 278, 157–180.
Leclerc, S.S., Rice, F.L., Dykes, R.W., Pourmoghadam, K., Gomez, C.M., 1993. Electrophysiological examination of the representation of the face in the suprasylvian gyrus of the ferret: a correlative study with cytoarchitecture. Somatosens. Mot. Res. 10, 133–159.
Li, Y., Van Hooser, S.D., Mazurek, M., White, L.E., Fitzpatrick, D., 2008. Experience with moving visual stimuli drives the early development of cortical direction selectivity. Nature 456, 952–956.
Liang, Z., Liu, X., Zhang, N., 2015. Dynamic resting state functional connectivity in awake and anesthetized rodents. Neuroimage 104, 89–99.
Liu, Y., Liang, M., Zhou, Y., He, Y., Hao, Y., Song, M., Yu, C., Liu, H., Liu, Z., Jiang, T., 2008. Disrupted small-world networks in schizophrenia. Brain 131, 945–961.
Lu, H., Zou, Q., Gu, H., Raichle, M.E., Stein, E.A., Yang, Y., 2012. Rat brains also have a default mode network. Proc. Natl. Acad. Sci. USA 109, 3979–3984.
Manger, P.R., Masiello, I., Innocenti, G.M., 2002. Areal organization of the posterior parietal cortex of the ferret (Mustela putorius). Cereb. Cortex 12, 1280–1297.
Manger, P.R., Nakamura, H., Valentiniene, S., Innocenti, G.M., 2004. Visual areas in the lateral temporal cortex of the ferret (Mustela putorius). Cereb. Cortex 14, 676–689.
Manger, P.R., Engler, G., Moll, C.K., Engel, A.K., 2008. Location, architecture, and retinotopy of the anteromedial lateral suprasylvian visual area (AMLS) of the ferret (Mustela putorius). Vis. Neurosci. 25, 27–37.
Marlinski, V., McCrea, R.A., 2008. Coding of self-motion signals in ventro-posterior thalamus neurons in the alert squirrel monkey. Exp. Brain Res. 189, 463–472.
McLaughlin, D.F., Sonty, R.V., Juliano, S.L., 1998. Organization of the forepaw representation in ferret somatosensory cortex. Somatosens. Mot. Res. 15, 253–268.
Mechling, A.E., Hubner, N.S., Lee, H.L., Hennig, J., von Elverfeldt, D., Harsan, L.A., 2014. Fine-grained mapping of mouse brain functional connectivity with resting-state fMRI. Neuroimage 96, 203–215.
Meredith, M.A., Allman, B.L., 2015. Single-unit analysis of somatosensory processing in the core auditory cortex of hearing ferrets. Eur. J. Neurosci. 41, 686–698.
Minshew, N.J., Keller, T.A., 2010. The nature of brain dysfunction in autism: functional brain imaging studies. Curr. Opin. Neurol. 23, 124–130.
Miranda-Dominguez, O., Mills, B.D., Grayson, D., Woodall, A., Grant, K.A., Kroenke, C.D., Fair, D.A., 2014. Bridging the gap between the human and macaque connectome: a quantitative comparison of global interspecies structure-function relationships and network topology. J. Neurosci. 34, 5552–5563.
Monti, M.M., Lutkenhoff, E.S., Rubinov, M., Boveroux, P., Vanhaudenhuyse, A., Gosseries, O., Bruno, M.A., Noirhomme, Q., Boly, M., Laureys, S., 2013. Dynamic change of global and local information processing in propofol-induced loss and recovery of consciousness. PLoS Comput. Biol. 9, e1003271.
Olson, C.R., Musil, S.Y., 1992. Topographic organization of cortical and subcortical projections to posterior cingulate cortex in the cat: evidence for somatic, ocular, and complex subregions. J. Comp. Neurol. 324, 237–260.
Pan, W.J., Billings, J.C., Grooms, J.K., Shakil, S., Keilholz, S.D., 2015. Considerations for resting state functional MRI and functional connectivity studies in rodents. Front. Neurosci. 9, 269.
Poole, T.B., 1978. An analysis of social play in polecats (Mustelidae) with comments on the form and evolutionary history of the open mouth play face. Anim. Behav. 26, 36–49.
Raichle, M.E., 2015. The brain's default mode network. Annu. Rev. Neurosci. 38, 433–447.
Raichle, M.E., Snyder, A.Z., 2007. A default mode of brain function: a brief history of an evolving idea. Neuroimage 37 (1083–1090), 1097-1089.
Raichle, M.E., MacLeod, A.M., Snyder, A.Z., Powers, W.J., Gusnard, D.A., Shulman, G. L., 2001. A default mode of brain function. Proc. Natl. Acad. Sci. USA 98, 676–682.
Ramsay, A.M., Meredith, M.A., 2004. Multiple sensory afferents to ferret pseudosylvian sulcal cortex. Neuroreport 15, 461–465.
Rice, F.L., Gomez, C.M., Leclerc, S.S., Dykes, R.W., Moon, J.S., Pourmoghadam, K., 1993. Cytoarchitecture of the ferret suprasylvian gyrus correlated with areas containing multiunit responses elicited by stimulation of the face. Somatosens. Mot. Res. 10, 161–188.
Rockland, K.S., 1985. Anatomical organization of primary visual cortex (area 17) in the ferret. J. Comp. Neurol. 241, 225–236.
Room, P., Russchen, F.T., Groenewegen, H.J., Lohman, A.H., 1985. Efferent connections of the prelimbic (area 32) and the infralimbic (area 25) cortices: an anterograde tracing study in the cat. J. Comp. Neurol. 242, 40–55.
Roy, A., Osik, J.J., Ritter, N.J., Wang, S., Shaw, J.T., Fiser, J., Van Hooser, S.D., 2016. Optogenetic spatial and temporal control of cortical circuits on a columnar scale. J. Neurophysiol. 115, 1043–1062.
Rubinov, M., Sporns, O., 2010. Complex network measures of brain connectivity: uses and interpretations. Neuroimage 52, 1059–1069.
Sanz-Arigita, E.J., Schoonheim, M.M., Damoiseaux, J.S., Rombouts, S.A., Maris, E., Barkhof, F., Scheltens, P., Stam, C.J., 2010. Loss of 'small-world' networks in Alzheimer's disease: graph analysis of FMRI resting-state functional connectivity. PLoS One 5, e13788.
Sawada, K., Watanabe, M., 2012. Development of cerebral sulci and gyri in ferrets (Mustela putorius). Congenit. Anom. 52, 168–175.
Sellers, K.K., Bennett, D.V., Hutt, A., Frohlich, F., 2013. Anesthesia differentially modulates spontaneous network dynamics by cortical area and layer. J. Neurophysiol. 110, 2739–2751.
Sellers, K.K., Bennett, D.V., Hutt, A., Williams, J.H., Frohlich, F., 2015. Awake vs. anesthetized: layer-specific sensory processing in visual cortex and functional connectivity between cortical areas. J. Neurophysiol. 113, 3798–3815.
Sforazzini, F., Schwarz, A.J., Galbusera, A., Bifone, A., Gozzi, A., 2014. Distributed BOLD and CBV-weighted resting-state networks in the mouse brain. Neuroimage 87, 403–415.
Sheline, Y.I., Price, J.L., Yan, Z., Mintun, M.A., 2010. Resting-state functional MRI in depression unmasks increased connectivity between networks via the dorsal nexus. Proc. Natl. Acad. Sci. USA 107, 11020–11025.
Shih, Y.Y., Li, G., Muir, E.R., De La Garza, B.H., Kiel, J.W., Duong, T.Q., 2012. Pharmacological MRI of the choroid and retina: blood flow and BOLD responses during nitroprusside infusion. Magn Reson. Med. 68, 1273–1278.
Shih, Y.Y., Wang, L., De La Garza, B.H., Li, G., Cull, G., Kiel, J.W., Duong, T.Q., 2013. Quantitative retinal and choroidal blood flow during light, dark adaptation and flicker light stimulation in rats using fluorescent microspheres. Curr. Eye Res. 38, 292–298.
Smith, G.B., Sederberg, A., Elyada, Y.M., Van Hooser, S.D., Kaschube, M., Fitzpatrick, D., 2015. The development of cortical circuits for motion discrimination. Nat. Neurosci. 18, 252–261.
Smith, S.M., Fox, P.T., Miller, K.L., Glahn, D.C., Fox, P.M., Mackay, C.E., Filippini, N., Watkins, K.E., Toro, R., Laird, A.R., Beckmann, C.F., 2009. Correspondence of the brain's functional architecture during activation and rest. Proc. Natl. Acad. Sci. USA 106, 13040–13045.
Spetsieris, P.G., Ko, J.H., Tang, C.C., Nazem, A., Sako, W., Peng, S., Ma, Y., Dhawan, V., Eidelberg, D., 2015. Metabolic resting-state brain networks in health and disease. Proc. Natl. Acad. Sci. USA 112, 2563–2568.
Spreafico, R., Barbaresi, P., Weinberg, R.J., Rustioni, A., 1987. SII-projecting neurons in the rat thalamus: a single- and double-retrograde-tracing study. Somatosens. Res. 4, 359–375.
Stafford, J.M., Jarrett, B.R., Miranda-Dominguez, O., Mills, B.D., Cain, N., Mihalas, S., Lahvis, G.P., Lattal, K.M., Mitchell, S.H., David, S.V., Fryer, J.D., Nigg, J.T., Fair, D.A., 2014. Large-scale topology and the default mode network in the mouse connectome. Proc. Natl. Acad. Sci. USA 111, 18745–18750.
Town, S.M., Atilgan, H., Wood, K.C., Bizley, J.K., 2015. The role of spectral cues in timbre discrimination by ferrets and humans. J. Acoust. Soc. Am. 137, 2870–2883.
Trezza, V., Campolongo, P., Vanderschuren, L.J., 2011. Evaluating the rewarding nature of social interactions in laboratory animals. Dev. Cogn. Neurosci. 1, 444–458.
Uehara, T., Yamasaki, T., Okamoto, T., Koike, T., Kan, S., Miyauchi, S., Kira, J., Tobimatsu, S., 2014. Efficiency of a "small-world" brain network depends on consciousness level: a resting-state FMRI study. Cereb. Cortex 24, 1529–1539.
van den Heuvel, M.P., Hulshoff Pol, H.E., 2010. Exploring the brain network: a review on resting-state fMRI functional connectivity. Eur. Neuropsychopharmacol. 20, 519–534.
Vincent, J.L., Patel, G.H., Fox, M.D., Snyder, A.Z., Baker, J.T., Van Essen, D.C., Zempel, J. M., Snyder, L.H., Corbetta, M., Raichle, M.E., 2007. Intrinsic functional architecture in the anaesthetized monkey brain. Nature 447, 83–86.
Vogt, B.A., Gabriel, M., 1993. Neurobiology of cingulate cortex and limbic thalamus: a comprehensive handbook, Boston: Birkhäuser.
Wang, H., Zeng, L.L., Chen, Y., Yin, H., Tan, Q., Hu, D., 2015. Evidence of a dissociation pattern in default mode subnetwork functional connectivity in schizophrenia. Sci. Rep. 5, 14655.
Watts, D.J., Strogatz, S.H., 1998. Collective dynamics of 'small-world' networks. Nature 393, 440–442.
Yu, C., Sellers, K.K., Radtke-Schuller, S., Lu, J., Xing, L., Ghukasyan, V., Li, Y., Shih, Yl., Murrow, R., Frohlich, F., 2015. Structural and functional connectivity between the lateral posterior-pulvinar complex and primary visual cortex in the ferret. Eur. J. Neurosci.
Zerbi, V., Grandjean, J., Rudin, M., Wenderoth, N., 2015. Mapping the mouse brain with rs-fMRI: an optimized pipeline for functional network identification. Neuroimage 123, 11–21.
Zhang, J., Wang, J., Wu, Q., Kuang, W., Huang, X., He, Y., Gong, Q., 2011. Disrupted brain connectivity networks in drug-naive, first-episode major depressive disorder. Biol. Psychiatry 70, 334–342.
Zhao, X., Liu, Y., Wang, X., Liu, B., Xi, Q., Guo, Q., Jiang, H., Jiang, T., Wang, P., 2012. Disrupted small-world brain networks in moderate Alzheimer's disease: a resting-state FMRI study. PLoS One 7, e33540.
Zhou, H., Schafer, R.J., Desimone, R., 2016a. Pulvinar-cortex interactions in vision and attention. Neuron 89, 209–220.
Zhou, Z.C., Yu, C., Sellers, K.K., Frohlich, F., 2016b. Dorso-lateral frontal cortex of the ferret encodes perceptual difficulty during visual discrimination. Sci. Rep. 6, 23568.